

*promoting access to White Rose research papers*



**Universities of Leeds, Sheffield and York**  
**<http://eprints.whiterose.ac.uk/>**

---

This is an author produced version of a paper published in **Geophysical & Astrophysical Fluid Dynamics**.

White Rose Research Online URL for this paper:  
<http://eprints.whiterose.ac.uk/4729/>

---

**Published paper**

Sreenivasan, B. and Gubbins, D. (2008) *Dynamos with weakly convecting outer layers: implications for core-mantle boundary interaction*. *Geophysical & Astrophysical Fluid Dynamics*, 102 (4). pp. 395-407.

---

# Dynamos with weakly convecting outer layers: implications for core-mantle boundary interaction

BINOD SREENIVASAN<sup>1</sup> and DAVID GUBBINS

School of Earth and Environment, University of Leeds, Leeds LS2 9JT, United Kingdom

*(Received 1 May 2007; in final form 5 October 2007)*

## Abstract

Convection in the Earth's core is driven much harder at the bottom than the top. This is partly because the adiabatic gradient steepens towards the top, partly because the spherical geometry means the area involved increases towards the top, and partly because compositional convection is driven by light material released at the lower boundary and remixed uniformly throughout the outer core, providing a volumetric sink of buoyancy. We have therefore investigated dynamo action of thermal convection in a Boussinesq fluid contained within a rotating spherical shell driven by a combination of bottom and internal heating or cooling. We first apply a homogeneous temperature on the outer boundary in order to explore the effects of heat sinks on dynamo action; we then impose an inhomogeneous temperature proportional to a single spherical harmonic  $Y_2^2$  in order to explore core-mantle interactions. With homogeneous boundary conditions and moderate Rayleigh numbers, a heat sink reduces the generated magnetic field appreciably; the magnetic

---

<sup>1</sup>Corresponding author; e-mail: earbs@earth.leeds.ac.uk

Reynolds number remains high because the dominant toroidal component of flow is not reduced significantly. The dipolar structure of the field becomes more pronounced as found by previous authors. Increasing the Rayleigh number yields a regime in which convection inside the tangent cylinder is strongly affected by the magnetic field. With inhomogeneous boundary conditions a heat sink promotes boundary effects and locking of the magnetic field to boundary anomalies. We show that boundary locking is inhibited by advection of heat in the outer regions. With uniform heating the boundary effects are only significant at low Rayleigh numbers, when dynamo action is only possible for artificially low magnetic diffusivity. With heat sinks the boundary effects remain significant at higher Rayleigh numbers provided the convection remains weak or the fluid is stably stratified at the top. Dynamo action is driven by vigorous convection at depth while boundary thermal anomalies dominate in the upper regions. This is a likely regime for the Earth's core.

**Keywords:** Geodynamo, core-mantle interaction, Earth's core, heat sink.

## 1 Background

In two earlier papers, hereafter referred to as I (Gubbins *et al.* 2007) and II (Willis *et al.* 2007), we have explored dynamo action in a fluid contained within a rotating, spherical annulus and cooled by imposing a laterally varying heat flux on the outer boundary. Of particular interest is the regime in which the fluid flow and magnetic field become locked to the boundary anomalies because this can explain the observation of the four relatively stationary main concentrations of flux seen on the surface of the Earth's core. Both papers used the pattern of seismic shear wave velocity at the base of the Earth's mantle for the heat flow boundary condition, in common with several previous studies (Glatzmaier *et al.* 1999, Bloxham 2000, Olson and Christensen 2002, Christensen and Olson 2003). Paper I found a near-steady solution with surface magnetic flux concentrated into four main lobes

located very close to those in the Earth. Paper II explored the parameter ranges required to produce quasi-steady solutions locked to the boundary. Factors controlling locking are the congruence of length scales, where the underlying convection with homogeneous boundary conditions must have length scales comparable to those of the inhomogeneous boundary conditions, and the state of convection in the fluid core, which must be such that thermal diffusion is effective in allowing the boundary anomalies to diffuse into the core and organize the internal flow. The latter required turbulent thermal diffusivity to be one order of magnitude higher than the magnetic diffusivity, which is unrealistic for the Earth. In this paper, therefore, we explore another regime that allows penetration of boundary inhomogeneities into the upper regions of the fluid core – we change the basic heating mode to produce vigorous convection at depth, but much reduced convection, or even stable stratification, in the upper core. This approach reduces the Péclet number in the upper regions without altering the deep convection significantly, thereby promoting boundary effects.

Several arguments have been put forward for the existence of weakened convection or a stratified layer at the top of the Earth’s outer core. Fearn and Loper (1981) suggested that light elements could rise through the core and accumulate in a thin layer beneath the core-mantle boundary (CMB). Gubbins *et al.* (1982) discussed the possibility of a thermally stratified layer developing over time as the Earth cooled. Another possible mechanism is an inward flux of buoyancy across the CMB (e.g. Lister and Buffett 1995, Olson 2000). Braginsky (1993) introduced a theory of the dynamics in a stratified upper core that he called the “hidden ocean of the core” and developed it in subsequent papers (Braginsky 1998, 1999, 2000). In a recent paper, Anufriev *et al.* (2005) consider the situation whereby the heat flux is superadiabatic at the inner core boundary (ICB) but subadiabatic at the CMB, which could have a significant effect on dynamo models. Stratification also eases problems with the Earth’s thermal history. The adiabat is steep and the core loses heat rapidly simply by cooling down the adiabat, so rapidly in fact that the inner core is thought

to have formed just 1 Gyr ago (Labrosse *et al.* 1997, Nimmo *et al.* 2004). Compositional convection plays an important, if not dominant, role in supplying buoyancy to drive the dynamo. The core might be thermally stable yet still convect vigorously all the way to the top, with compositional buoyancy maintaining mixing against the thermal stratification (Loper 1978).

The standard model of core convection assumes a cooling core that freezes at the ICB, releasing a light component of the liquid that rises. The light component is usually assumed to become mixed throughout the outer core, contributing to a slow secular decrease in its density. The equations are the same for compositional convection as for thermal convection, the only difference being in the diffusivity; double-diffusive effects have not been observed and are too exotic to have attracted much interest at this primitive stage of the theory. The counterpart of heat conduction down the adiabat is barodiffusion of the light component down the pressure gradient, which may be significant (Braginsky 1963), but composition becomes well mixed by convection so there is no equivalent to the adiabatic temperature gradient.

Here we adopt a model of thermal, Boussinesq convection, but use the standard core model to guide our choice of buoyancy sources. The Boussinesq temperature equation governs fluctuations about a basic temperature profile comprising the steady-state conduction solution minus the adiabat. This profile may well have a negative gradient for temperatures appropriate to the Earth's core, corresponding to heat sinks in the Boussinesq model. In reality there are no heat sinks in the core; they arise in the heat equation as a result of a subadiabatic conduction profile. In the special case when the adiabat has a quadratic form, which is a fair match to recent estimates of the adiabat (e.g. Gubbins *et al.* 2004), the equivalent heat sink is uniform – in general the adiabat will correspond to a radially dependent heat sink. The *real* heat sources, from radioactivity and secular cooling, must be added to this in the Boussinesq heat equation.

The mix of compositional and thermal buoyancy also provides a mix of sources at the

bottom (latent heat of freezing and release of light material at the ICB), internal heating (specific heat of cooling and radiogenic isotopes in the core), and heat sinks (subadiabatic regions and re-mixing of light material throughout the liquid core). We therefore adopt a simple basic temperature profile that includes both uniform internal heating (or cooling) and bottom heating, and retain the freedom to vary the relative importance of each.

We make two further simplifications over the model in Papers I and II. First, we replace the “tomographic” boundary condition based on seismic shear wave velocity with its dominant spherical harmonic  $Y_2^{2c}$  (e.g. Sarson *et al.* 1997). This function has minima around the great circle  $\phi = \pm\pi/2$ , mimicking the cold lower mantle beneath the Pacific rim where geomagnetic flux is concentrated. The effects of this simpler geometry should be easier to interpret. Secondly we use a temperature rather than a heat flux boundary condition. This simplifies interpretation because, with heat flux boundary conditions, the length scales of convection at the moderate Ekman numbers conveniently accessible numerically are a very sensitive function of the Ekman number (Gibbons *et al.* 2007), making it difficult to judge in advance whether or not a particular dynamo is likely to lock. With temperature boundary conditions the length scale dependence on the Ekman number is monotonic near onset of convection.

The paper is organized as follows. In the next section, we present the governing equations and parameters. In section 3 we present dynamo solutions with homogeneous boundary conditions and explore their dependence on the relevant governing parameters. In section 4 we include the inhomogeneous boundary condition and study regimes in which these dynamos lock. In both sections a comparative study is made of dynamos with weak and strong convection beneath the outer boundary. The paper concludes with a summary of results and consequences for geodynamo studies.

## 2 Governing equations and parameters

Consider an electrically conducting, Boussinesq fluid between two concentric, co-rotating spherical surfaces. The radius ratio  $r_i/r_o$  is 0.35. The temperatures of the inner and outer boundaries are kept fixed; otherwise the mathematical formulation of the problem and its numerical solution are as described in Paper II. The time-dependent MHD equations for the velocity  $\mathbf{u}$ , the magnetic field  $\mathbf{B}$  and the temperature  $T$  are

$$EPm^{-1}\left(\frac{\partial\mathbf{u}}{\partial t} + (\mathbf{u} \cdot \nabla)\mathbf{u}\right) + 2\mathbf{e}_z \times \mathbf{u} = -\nabla p + Ra\frac{\mathbf{r}}{r_o} Pm Pr^{-1}T + (\nabla \times \mathbf{B}) \times \mathbf{B} + E\nabla^2\mathbf{u}, \quad (1)$$

$$\frac{\partial\mathbf{B}}{\partial t} = \nabla \times (\mathbf{u} \times \mathbf{B}) + \nabla^2\mathbf{B}, \quad (2)$$

$$\frac{\partial T}{\partial t} + (\mathbf{u} \cdot \nabla)T = Pm Pr^{-1} \nabla^2 T + Q_D, \quad (3)$$

$$\nabla \cdot \mathbf{u} = \nabla \cdot \mathbf{B} = 0. \quad (4)$$

The dimensionless groups in the above equations are the Ekman number,  $E = \nu/\Omega L^2$ , the Prandtl number,  $Pr = \nu/\kappa$ , the ‘modified’ Rayleigh number,  $Ra = g\alpha\Delta T_b L/\Omega\kappa$ , and the magnetic Prandtl number,  $Pm = \nu/\eta$ . We shall refer to the product  $PmPr^{-1} = q = \kappa/\eta$  as the Roberts number, a measure of the strength of thermal diffusion relative to magnetic diffusion in the model. The uniform heat source (sink) density is represented by  $Q_D$  in (3). In the above expressions,  $L$  is the gap-width of the spherical shell,  $\Delta T_b$  is the temperature difference across the layer from basal heating,  $\nu$  is the kinematic viscosity,  $\kappa$  is the thermal diffusivity and  $\eta$  is the magnetic diffusivity. The unit of length is  $L$  and of time  $L^2/\eta$ . No-slip, electrically insulating boundaries are used as they permit comparison of our results with several previously published calculations.

We use three intrinsic dimensionless parameters. As velocity is scaled by  $\eta/L$ , the dimensionless mean velocity,  $uL/\eta$ , gives the magnetic Reynolds number,  $R_m$ . Magnetic field is measured in units of  $(\rho\Omega\mu\eta)^{1/2}$ ,  $\rho$  being the density and  $\mu$  the permeability of free space. The Elsasser number is therefore the square of the mean dimensionless magnetic

field,  $\overline{B}$ . As the competition between advection and thermal diffusion is expected to play a role in core-boundary coupling, the Péclet number,  $Pe = uL/\kappa$  is introduced as another intrinsic parameter in the model. The dimensionless kinetic and magnetic energies are given by

$$E_k = \frac{1}{2} \int \mathbf{u}^2 dV, \quad E_m = \frac{Pm}{2E} \int \mathbf{B}^2 dV;$$

both are scaled up to their true value when multiplied by  $\rho\eta^2/L^2$ .

The basic state temperature profile has the form

$$T_0(r) = -\frac{1}{2}\beta_i r^2 + \frac{\beta_b}{r}; \quad \beta_i = Q_D/3q, \quad (5)$$

where  $\beta_i$  and  $\beta_b$  are constants representing intrinsic and basal heating respectively. In our study,  $\beta_b$  is kept fixed at  $r_i r_o$  so that the temperature difference from basal heating,  $\Delta T_b$  is unity in dimensionless units. The desired intrinsic heating (cooling) is obtained by varying  $\beta_i$  in the model. Following the definition of the Rayleigh number,  $Ra$ , based on  $\Delta T_b$ , we define an independent Rayleigh number,  $Ra_i$ , based on the temperature difference corresponding to internal heating (cooling):

$$Ra_i = \frac{g\alpha\Delta T_i L}{\Omega\kappa}, \quad (6)$$

where  $\Delta T_i = (Q_D/6q)(r_o^2 - r_i^2)$ . Note that  $Ra_i$  would be negative for a volumetric heat sink.

The total temperature,  $T$ , is expressed as the sum of the basic temperature and a fluctuating component:

$$T(r, \theta, \phi, t) = T_0(r) + T_1(r, \theta, \phi, t).$$

Subtracting  $T_0(r)$  from  $T$  in equation (3) leaves an equation for the temperature perturbation  $T_1$  with no heat source term. Inhomogeneous temperature outer boundary conditions are introduced in section 4. The temperature perturbation  $T_1$  is then decomposed into a homogeneous part,  $\Theta$  and a fixed inhomogeneous part,  $f$  such that

$$T_1 = \Theta(r, \theta, \phi, t) + fY_2^{2c}(\theta, \phi). \quad (7)$$

where  $Y_2^{2c}$  is a Schmidt-normalised spherical harmonic with maxima at  $\phi = 0, \pm\pi$  and minima at  $\phi = \pm\pi/2$  and  $f$  is the amplitude of the inhomogeneity. Since temperature is kept fixed at both boundaries in this study,  $\Theta(r_i) = \Theta(r_o) = 0$ . To quantify the inhomogeneity at the outer boundary, another Rayleigh number,  $Ra_H$ , is defined based on the maximum (peak-to-peak) temperature variation at the outer boundary,  $\Delta T_H$ .

The Rayleigh number  $Ra$  is varied between approximately 10 and 20 times its critical value for the onset of nonmagnetic convection. This is one order of magnitude higher than the Rayleigh numbers considered in Papers I & II. For the parameter ranges considered in the next two sections, the maximum spherical harmonic degree must be at least 60 and 60–80 grid points are used in the radial direction. All calculations reported in this paper have been performed at  $E = 10^{-4}$ .

### 3 Dynamo action with homogeneous boundary conditions

A summary of the results with homogeneous boundaries are given in table 1. For Rayleigh numbers of  $Ra = 750$  and 1000, a heat sink decreases  $R_m$  only slightly but the average magnetic field ( $\overline{B}$ , obtained from the magnetic energy in the spherical shell) registers a sharp decrease. For a strong heat sink ( $Ra_i = -519$ ), the poloidal kinetic energy decreases but the toroidal energy does not; approximately 80% of the kinetic energy is contained in the toroidal component (table 1). The decrease in  $R_m$  is due to the fall in poloidal velocity; note that  $u_r$  is very small in the outer periphery of the spherical shell in figure 2(b) (also see table 2). Convection is shut down in the outer regions and this is reflected in the overall magnetic field generated in the shell. The ratio of magnetic to kinetic energies decreases to unity as  $Ra_i$  is reduced. Reducing  $Ra_i$  further results in failure of dynamo action.

Increasing the Rayleigh number to a higher value ( $Ra = 1750$ ) gives rise to additional effects that are not observed at moderate Rayleigh numbers – the buoyancy forces now are large enough to generate a large-scale zonal motion, whereby the  $m = 0$  mode is strong in the kinetic energy spectrum; see figure 4(a). From figure 4(b) we note that the heat sink acts in two ways: (i) to reduce energy in the  $m = 0$  mode and (ii) to damp out energy contained in high azimuthal wave modes (small scales). The latter effect is also present at moderate Rayleigh numbers ( $Ra = 750$ ) as is clear from a comparison of two cases given in figures 2(a,b). Hence the fall in kinetic energy (and  $R_m$ ) caused by the heat sink is greater at high Rayleigh numbers than at low or moderate Rayleigh numbers. Consequently, the ratio of magnetic to kinetic energies is not affected much (see table 1, cases 7 & 8).

Cases 2 & 5 in table 1 are equivalent in the sense that, the magnetic Reynolds number, the mean magnetic field and the energy contained in the toroidal component are all approximately the same. This is not surprising if we note that the sum of the Rayleigh numbers based on basal heating and internal cooling,  $Ra + Ra_i$ , is approximately the same for the two cases. The main difference between these two states is in the heat flux at the outer boundary: in case 5 the heat flux is lower due to the presence of the heat sink. From table 2 we see that the reduced heat flux at the outer boundary has a small but finite effect on the radial velocity distribution in the fluid core, the upwelling velocity in the outer regions being lower and of the same order of magnitude as the downwelling velocity. When the effect of the heat sink is dominant (case 4, table 2), the radial velocity decreases to a low value with increasing radius.

Separating the kinetic and magnetic energies into parts symmetric and antisymmetric about the equator shows that the solution becomes progressively symmetric as  $Ra_i$  decreases and for the minimum values the solution has near-perfect symmetry about the equator. Furthermore, as  $Ra_i$  is reduced, the field structure is a stable dipole [figure 1(b)], qualitatively similar to the results of Kutzner and Christensen (2002), who used volumet-

ric heat sinks to mimic chemical convection in their dynamo. (See Wicht and Olson (2004) and Christensen (2006) for further examples of the application of heat sinks in chemical convection.)

Figure 1(a) shows reverse-flux patches (of sign opposite to that of the main dipole field) at low latitudes. These are common in many geodynamo simulations (also see Olson *et al.* 1999, Sreenivasan and Jones 2006b), but they are absent from the runs with an imposed heat sink: for the lowest  $Ra_i$  these flux patches are eliminated totally from the outer boundary [figure 1(b)]. From figure 2(c) we see discontinuities in the toroidal magnetic field in regions of strong downwelling.  $B_\phi$  is twisted by the shear  $\partial u_r / \partial \phi$  to give a negative  $B_r$  above the equatorial plane [figure 2(d)], but the phenomenon now occurs deep within the shell and hence is not visible on the outer boundary.

A strong heat sink also changes the mode of convection in the tangent cylinder – the imaginary cylinder touching the inner core boundary and parallel to the Earth’s rotation axis. Flow dominated by a strong upwelling plume as in figure 3(a) (called the magnetic mode, see Sreenivasan and Jones 2006a) changes to a regime where there are several thin, weak upwellings [the viscous mode; see figure 3(b)]. As convection is damped out, the maximum Elsasser number within the tangent cylinder falls below the value required for the magnetic mode of convection. The expulsion of magnetic flux and the formation of reverse flux patches in the tangent cylinder requires the strong upwellings that we associate with the magnetic mode. However, in case 8 the convection within the tangent cylinder is again strong enough to excite the magnetic mode [figure 3(c)]. Here we have a regime wherein convection is vigorous in the bulk of the fluid but weak enough in the outer regions to preclude the occurrence of reverse flux patches near the equatorial plane [see figure 1(c)]. We note from table 1 that the heat flux at the outer boundary is very small in this regime.

## 4 Dynamo action with inhomogeneous boundary conditions: locking

Now consider the same problem as in the previous section but with the temperature outer boundary condition of the form  $T(r_o) = fY_2^2(\theta, \phi)$ . Figure 5 gives the velocity and magnetic field plots for case 1, table 3. The parameters for this run are  $Ra = 1000$ ,  $Ra_i = -249$ . When the temperature inhomogeneity is small there is no perceivable effect on the dynamo and multi-columnar convection is dominant. With  $Ra_H \approx 2500$  convection is organized into two strong downwellings beneath regions of low temperature [see figures 5(a,b)]. These two downwellings remain close to the same longitude during one run. Although the magnitude of the magnetic field fluctuates with time, the four-lobed structure of the radial magnetic field as seen in figures 5(c) and (d) is preserved at approximately the same longitude throughout the run. As the kinetic and magnetic energy spectra decay by three orders of magnitude in our calculations, the small-scale structures in figures 5(a) and (c) are well-resolved parts of the solution. Case 2 ( $Ra = 1750$ ,  $Ra_i = -909$ ,  $Ra_H \approx 3000$ ) has strong convection that gives rise to weak or even reversed flux patches in both hemispheres. Despite the chaotic nature of the solution, the magnetic field shows the  $m = 2$  pattern of the inhomogeneity. The magnetic Reynolds number and Elsasser number ( $\overline{B}^2$ ) of this dynamo are comparable to those in case 1.

As  $Ra_i$  is increased to zero and positive values, the outer surface temperature in the dynamo progressively decreases, the mean heat flux at the boundary increases, and convection decouples from the boundary temperature variations. For  $Ra_i = +78$  (i.e. with a heat source rather than a heat sink), dipolar solutions were obtained with  $Ra_H = 0$  but the behaviour is different for  $Ra_H \sim 800$ : the dipolar structure of the magnetic field breaks down into a chaotic state. The magnetic energy decreases to only a fraction of the kinetic energy (case 3, table 3). This regime is reminiscent of the low  $Pr = Pm$  regime of Sreenivasan and Jones (2006b) where the Lorentz forces do not play a significant part in

the force balance. Runs at higher values of  $Ra$  or  $Ra_i$  were not attempted as they would produce only non-dipolar dynamos.

We explore two ways to force a locked solution when convection is strong: (i) to increase  $Ra_H$ , keeping  $q = \kappa/\eta$  equal to unity and (ii) to decrease  $Ra$  and increase  $q$ . The first option (case 4 in table 3) is effective in forcing two strong downwellings, producing a strong dipolar magnetic field as shown in figures 6(a,b). However, prograde (eastward) thermal winds beneath the boundary tend to tilt the fluid columns and, at higher values of  $Ra_H$ , destroy both the columnar convection and the dynamo. A similar effect was observed with  $Y_2^2$  and  $Y_2^0$  heat flow patterns by Olson and Christensen (2002). This places an upper limit on the useable value of  $Ra_H$ . When stronger heat sources are present it becomes more difficult to produce locked dynamos by increasing  $Ra_H$  as the regime narrows down. However, increasing  $q$  to 8 [option (ii) above; see case 5 in table 3 and figures 6(c,d)] and lowering  $Ra$  to 125 restores the solution with quasi-stationary flux lobes. This result is significant because it indicates that the key to obtaining locked solutions is to create a regime where external thermal perturbations can penetrate into the interior of the fluid. This requires a small Péclet number,  $uL/\kappa$ , which is 38 for case 5 compared with 213 for case 1.

## 5 Discussion

We have obtained dynamo solutions where convection is weakened in the upper regions of the fluid by a basic state temperature distribution that incorporates both boundary heat flux and uniform internal cooling. This regime cannot be obtained by merely reducing the Rayleigh number in a model with only uniform internal heating and does not preclude strong convection from occurring lower down in the fluid. Models with moderate Rayleigh numbers and strong heat sinks (case 4 of table 1) give rise to severe thermal stratification with net heat flux into the outer boundary. The temperature gradient changes sign at

$r = 1.183$ ; the surface heat flux is still inwards but is less than that for the basic state (table 1), indicating that convection still occurs throughout the fluid. The equivalent situation in the Earth's core would be a conduction profile that becomes subadiabatic 800 km below the CMB and a positive, but subadiabatic heat flow out of the core. The magnetic energy is considerably attenuated and the dynamos are stable and dipolar. Here we have shown that such models support strong thermal boundary coupling even when  $q = \kappa/\eta \sim 1$ .

Papers I and II used uniform internal heating, which meant the heat flux was highest at the top. This forced vigorous advection of heat near the upper boundary, which swamped any influence of the lateral variations of heat flux on the boundary except at small Rayleigh number. This entailed weak convective velocities everywhere, producing a small magnetic Reynolds number and little hope of dynamo action unless the magnetic diffusivity was reduced, which in terms of dimensionless parameters meant, inevitably, a large  $q$ . Molecular values for the core suggest  $q \approx 10^{-6}$ , but this is irrelevant for the type of turbulence expected in the core. Turbulence is usually assumed to equalise the diffusivities, making  $q \approx 1$ , but large  $q$  of order 10 is unreasonable. In this paper we obviate the need for large  $q$  by introducing heat sinks that reduce the advection of heat near the upper boundary, allowing lateral heat flux variations at the boundary to influence the deeper convection and produce locking at higher Rayleigh number. These heat sinks are eminently realistic for modelling the core for two reasons. First, convection is driven only by the superadiabatic temperature gradient, which is weakened towards the CMB by the steepening of the adiabatic gradient. Secondly, compositional convection, which provides most of the buoyancy in the core, is fed from the bottom in the form of light material released on freezing of the liquid and is remixed uniformly throughout the outer core.

The solutions obtained here are more mobile than the case with the largest inhomogeneity in Paper I and are not as well locked. They are no less geophysically relevant for

this because the geomagnetic field is also mobile. Surface fields are dominated by 4 main lobes that move irregularly a small distance from the mean position of the locked solutions. A preliminary exploration into lower Ekman numbers ( $\sim 10^{-5}$ ) suggests locking continues to occur at high Rayleigh numbers when heat sinks are present.

## 6 Acknowledgements

This work was supported by NERC Consortium Grant *Deep Earth Systems* O/2001/00668 and Grant F/00 122/AD from the Leverhulme Trust. The computations were performed on the White Rose Grid Cluster at Leeds University.

## References

- Anufriev, A. P., Jones, C. A., and Soward, A. M., The Boussinesq and anelastic liquid approximation for convection in the Earth's core. *Phys. Earth Planet. Inter.*, 2005, **152**, 163–190.
- Bloxham, J., The effect of thermal core-mantle interactions on the paleomagnetic secular variation. *Phil. Trans. Roy. Soc. London Ser. A*, 2000, **358**, 1171–1179.
- Braginsky, S. I., Structure of the F layer and reasons for convection in the Earth's core. *Dokl. Akad. Nauk. SSSR Engl. Trans.*, 1963, **149**, 1311–1314.
- Braginsky, S. I., MAC-oscillations of the hidden ocean of the core. *J. Geomagn. Geoelectr.*, 1993, **45**, 1517–1538.
- Braginsky, S. I., Magnetic Rossby waves in the stratified ocean of the core, and topographic core-mantle coupling. *Earth Planets Space*, 1998, **50**, 641–649.

- Braginsky, S. I., Dynamics of the stably stratified ocean at the top of the core. *Phys. Earth Planet. Inter.*, 1999, **111**, 21–934.
- Braginsky, S. I., Effect of the stratified ocean of the core upon the Chandler wobble. *Phys. Earth Planet. Inter.*, 2000, **118**, 195–203.
- Christensen, U. R., A deep dynamo generating mercury’s magnetic field. *Nature*, 2006, **444**, 1056–1058.
- Christensen, U. R. and Olson, P., Secular variation in numerical geodynamo models with lateral variations of boundary heat flow. *Phys. Earth Planet. Inter.*, 2003, **138**, 39–54.
- Fearn, D. R. and Loper, D. E., Compositional convection and stratification of Earth’s core. *Nature*, 1981, **289**, 393–394.
- Gibbons, S. J., Gubbins, D., and Zhang, K., Convection in a rotating spherical fluid shells with inhomogeneous heat flux at the outer boundary. *Geophys. Astrophys. Fluid Dynam.*, 2007, p. in press.
- Glatzmaier, G. A., Coe, R. S., Hongre, L., and Roberts, P. H., The role of the Earth’s mantle in controlling the frequency of geomagnetic reversals. *Nature*, 1999, **401**, 885–890.
- Gubbins, D., Thomson, C. J., and Whaler, K. A., Stable regions in the Earth’s liquid core. *Geophys. J. R. Astron. Soc.*, 1982, **68**, 241–251.
- Gubbins, D., Alfè, D., Masters, T. G., Price, D., and Gillan, M., Gross thermodynamics of 2-component core convection. *Geophys. J. Int.*, 2004, **157**, 1407–1414.
- Gubbins, D., Willis, A. P., and Sreenivasan, B., Correlation of Earth’s magnetic field with lower mantle thermal and seismic structure. *Phys. Earth Planet. Inter.*, 2007, **162**, 256–260.

- Kutzner, C. and Christensen, U., From stable dipolar towards reversing numerical dynamos. *Phys. Earth Planet. Inter.*, 2002, **131**, 29–45.
- Labrosse, S., Poirier, J.-P., and Mouël, J.-L. L., On cooling of the Earth’s core. *Phys. Earth Planet. Inter.*, 1997, **99**, 1–17.
- Lister, J. R. and Buffett, B. A., The strength and efficiency of thermal and compositional convection in the geodynamo. *Phys. Earth Planet. Inter.*, 1995, **91**, 17–30.
- Loper, D. E., Some thermal consequences of a gravitationally powered dynamo. *J. Geophys. Res.*, 1978, **83**, 5961–5970.
- Nimmo, F., Price, G., Brodholt, J., and Gubbins, D., The influence of potassium on core and geodynamo evolution. *Geophys. J. Int.*, 2004, **156**, 1407–1414.
- Olson, P., Thermal interaction of the core and mantle. In: *Earth’s Core and Lower Mantle*, C. Jones, A. Soward, and K. Zhang (Eds), pp. 1–38, 2000 (London: Taylor and Francis).
- Olson, P. and Christensen, U. R., The time-averaged magnetic field in numerical dynamos with non-uniform boundary heat flow. *Geophys. J. Int.*, 2002, **151**, 809–823.
- Olson, P., Christensen, U., and Glatzmaier, G., Numerical modeling of the geodynamo: mechanisms of field generation and equilibration. *J. Geophys. Res.*, 1999, **104**, 10,383–10,404.
- Sarson, G. R., Jones, C. A., and Longbottom, A. W., The influence of boundary region heterogeneities on the geodynamo. *Phys. Earth Planet. Inter.*, 1997, **101**, 13–32.
- Sreenivasan, B. and Jones, C. A., Azimuthal winds, convection and dynamo action in the polar regions of planetary cores. *Geophys. Astrophys. Fluid Dynam.*, 2006, **100**, 319–339.

- Sreenivasan, B. and Jones, C. A., The role of inertia in the evolution of spherical dynamos. *Geophys. J. Int.*, 2006, **164**, 467–476.
- Wicht, J. and Olson, P., A detailed study of the polarity reversal mechanism in a numerical dynamo model. *Geochem. Geophys. Geosyst.*, 2004, **5**, Q03H10.
- Willis, A. P., Sreenivasan, B., and Gubbins, D., Thermal core-mantle interaction: exploring regimes for ‘locked’ dynamo action. *Phys. Earth Planet. Inter.*, 2007, **165**, 83–92.

No.	$Ra$	$Ra_i$	$R_m$	$\%E_{k,tor}$	$\overline{B}$	$E_m/E_k$	$\partial T_0/\partial r _{r_o}$	$\partial T/\partial r _{r_o}$
1	750	+78	94.4	0.696	1.72	16.61	-0.5038	-1.429
2	750	0	84.0	0.701	1.35	15.72	-0.35	-1.104
3	750	-156	77.2	0.69	0.95	2.3	-0.0423	-0.547
4	750	-389	57.6	0.78	0.468	1.006	+0.4192	+0.23
5	1000	-249	83.6	0.719	1.55	17.38	+0.0192	-0.524
6	1000	-519	73.5	0.79	0.536	2.66	+0.4192	+0.18
7	1750	-413	139.4	0.68	2.2	26.04	0.0	-1.02
8	1750	-909	96.9	0.73	1.57	26.08	+0.4192	-0.0132

Table 1: Summary of the regimes with homogeneous boundaries.  $Pr = Pm = 5$  in all runs except for  $Ra = 1750$ , where  $Pr = Pm = 10$ .  $\partial T_0/\partial r$  is the conductive heat flux and  $\partial T/\partial r$  is the net heat flux.

No.	$Ra$	$Ra_i$	$u_r(r = 0.6r_o)$	$u_r(r = 0.75r_o)$	$u_r(r = 0.9r_o)$	$u_r(r = 0.95r_o)$
2	750	0.0	[-246, 215]	[-223, 212]	[-168, 194]	[-115, 142]
5	1000	-249	[-259, 183]	[-246, 155]	[-180, 161]	[-119, 121]
4	750	-389	[-125, 81]	[-70, 50]	[-36, 33]	[-19, 17]

Table 2: Ranges of radial velocities at four different radii in the fluid core for three of the cases in Table 1.

No.	$q$	$Ra$	$Ra_i$	$\Delta T_H$	$Ra_H$	$R_m$	$E_m/E_k$	$\partial T/\partial r _{r_o}$	Locking
1	1.0	1000	-249	2.466	2466	213	3.56	-2.066	Yes
2	1.0	1750	-909	1.695	2966	227	7.45	-0.8802	Yes
3	1.0	750	+78	1.051	788	158	0.346	-1.876	No
4	1.0	750	+78	3.360	2520	225	3.69	-3.570	Yes
5	8.0	125	+78	1.552	194	306	14.62	-1.022	Yes

Table 3: Summary of the regimes considered with lateral variation in boundary temperature. All calculations are at  $E = 10^{-4}$ .

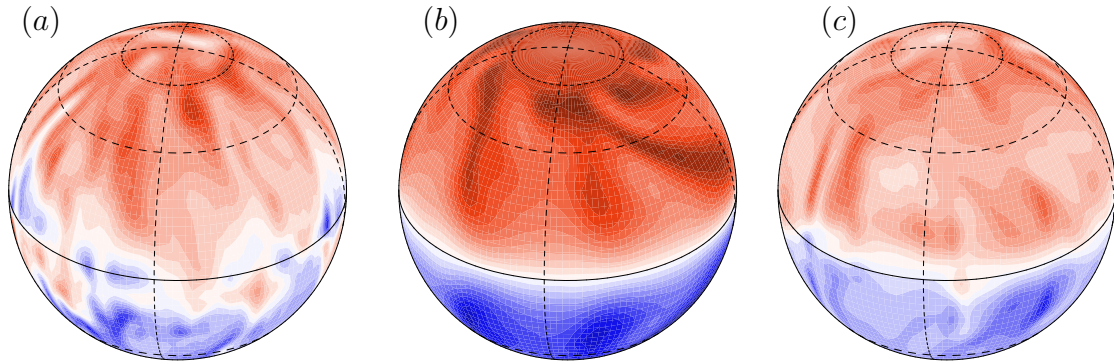


Figure 1: Shaded contour plots of the radial magnetic field ( $B_r$ ) at the outer boundary  $r = r_o$  for dynamos with the parameters (a)  $Ra_i = 0$ ,  $Ra = 750$ , (b)  $Ra_i = -389$ ,  $Ra = 750$  and (c)  $Ra_i = -909$ ,  $Ra = 1750$ . The maximum and minimum values for the plots are (a)  $[-1.094, 0.794]$ , (b)  $[-0.1704, 0.1704]$  and (c)  $[-1.297, 0.803]$ . Positive values are shown in red and negative values in blue; see the online version for colour. The thick dashed line gives the latitude where the tangent cylinder cuts the outer boundary, and the thin dashed line represents latitude  $45^\circ$  N. The dashed vertical lines correspond to longitudes spaced  $90^\circ$  apart.

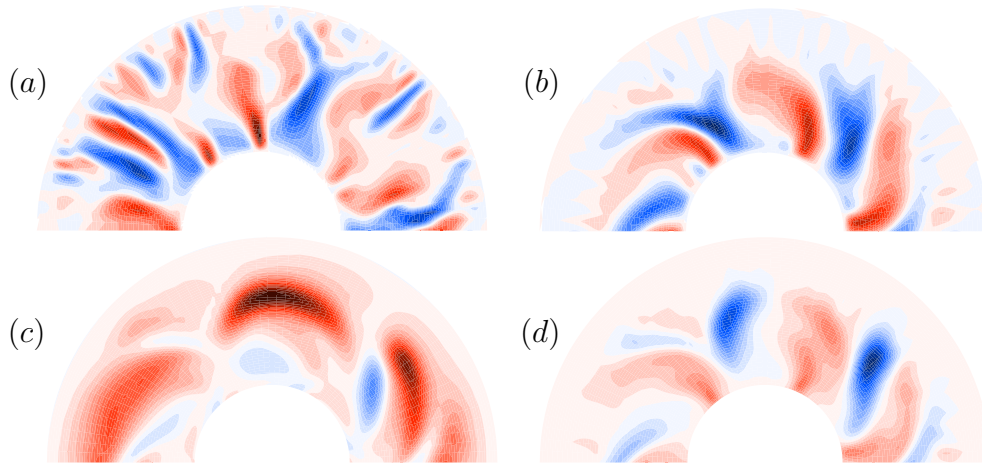


Figure 2: (a) & (b): Shaded contour plots of the radial velocity at the horizontal section  $z = 0$  (equatorial plane) for a dynamo with  $Ra = 750$ ,  $Ra_i = +78$  &  $Ra_i = -389$ . Regions in red show positive (upwelling) velocities and blue regions show downwellings; see the online version for colour. (c) & (d): Contours of the azimuthal and radial magnetic fields at the section  $z = 0.1$  above the equatorial plane, for  $Ra = 750$ ,  $Ra_i = -389$ . The ranges of values for the plots are (a)  $[-238, 299.16]$ , (b)  $[-119.54, 93.64]$ , (c)  $[-0.654, 1.664]$  and (d)  $[-1.25, 0.58]$ .

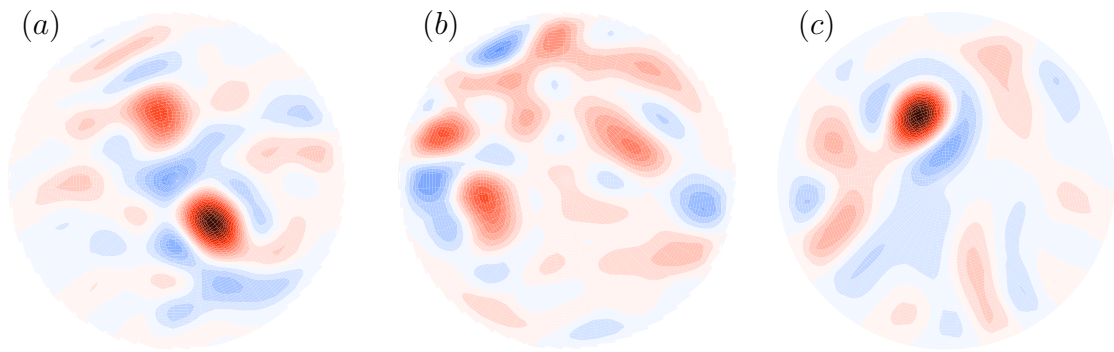


Figure 3: Shaded contour plots of the radial velocity at the horizontal section  $z = 1.46$  above the equatorial plane for dynamos with (a)  $Ra = 1000$ ,  $Ra_i = -249$ , (b)  $Ra = 1000$ ,  $Ra_i = -519$ , and (c)  $Ra = 1750$ ,  $Ra_i = -909$ . This section has a radius 0.485 in dimensionless units and lies entirely within the tangent cylinder (radius 0.538). Regions in red show positive (upwelling) velocities and blue regions show downwellings (see the online version for colour). The ranges of values in the three plots are (a)  $[-32.2, 107.2]$ , (b)  $[-16.43, 23.9]$  and (c)  $[-21.26, 76.78]$ .

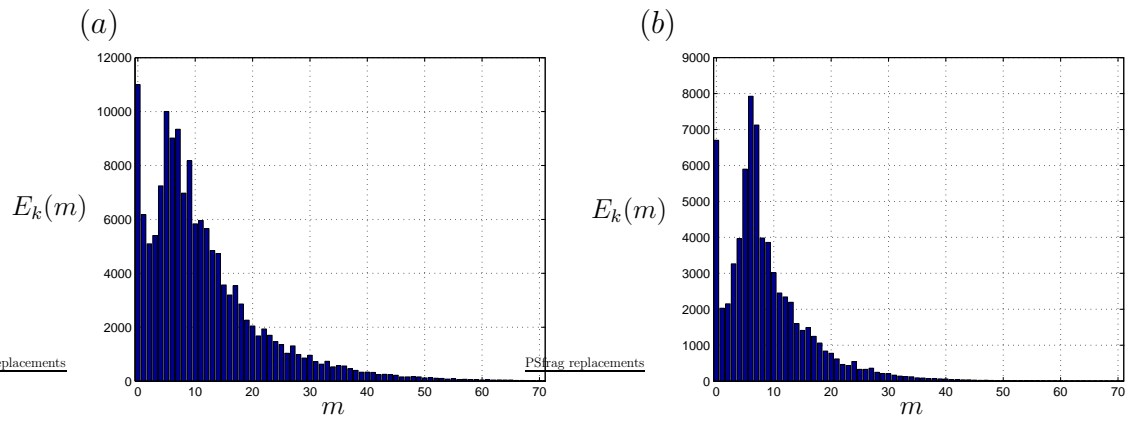


Figure 4: Time-averaged kinetic energy spectra showing decay over the harmonic order,  $m$ . The Rayleigh number,  $Ra = 1750$ . The cases shown are (a)  $Ra_i = -413$  and (b)  $Ra_i = -909$ .

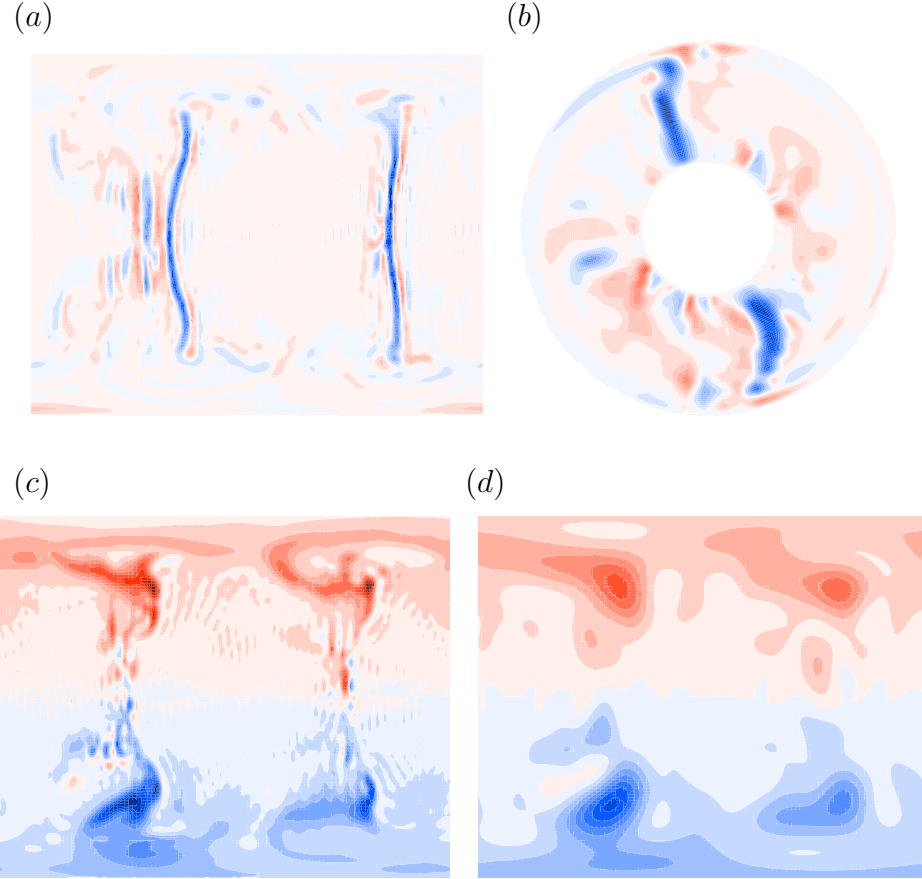


Figure 5: (a) Snapshot of the radial velocity on the spherical surface  $r = 0.8r_o$ . The horizontal axis covers the range  $-\pi < \phi < \pi$  in longitude and the vertical axis covers the range  $0 < \theta < \pi$  in colatitude. The range of values are  $[-647.5, 304.4]$ . (b) Radial velocity contours on the equatorial plane, with range  $[-772.5, 419.8]$ . (c) Radial magnetic field plot at the outer boundary,  $r = r_o$ . The range of values is  $[-1.6, 1.76]$ . (d) Radial magnetic field at  $r = r_o$ , truncated to spherical harmonic degree  $l = 14$ . The range of values is  $[-0.89, 0.95]$ . The parameters in the model are  $Ra = 1000$ ,  $E = 10^{-4}$ ,  $q = \kappa/\eta = 1$ ,  $Ra_H = 2466$ ,  $Ra_i = -249$ . Positive values are shown in red and negative values in blue.

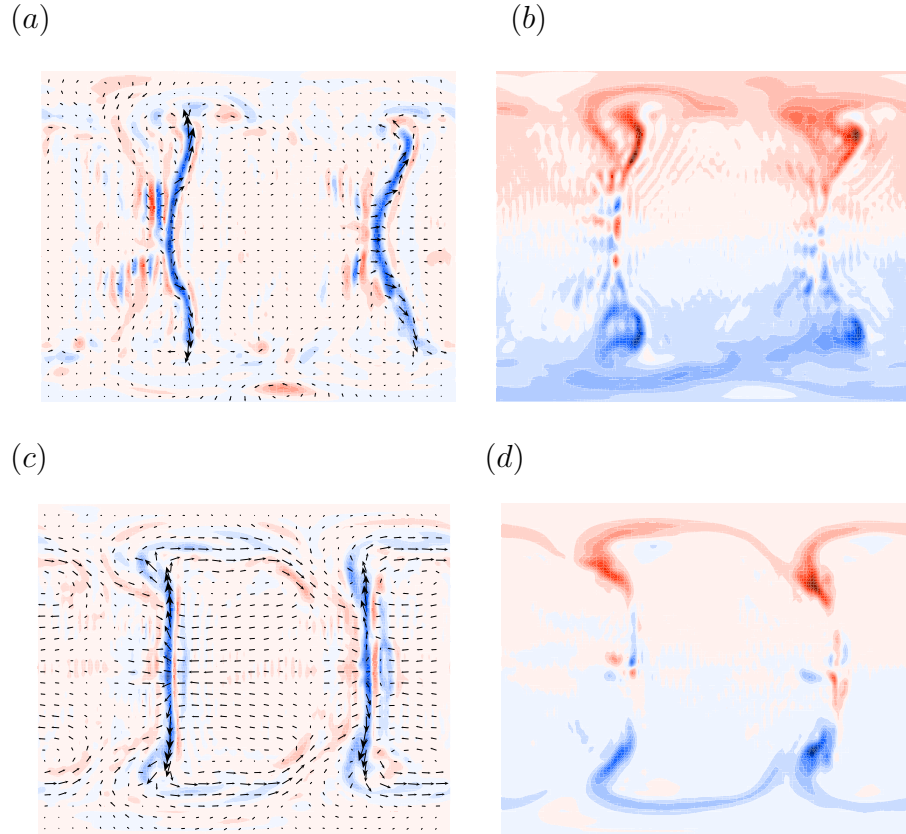


Figure 6: (a) & (b): Snapshots of  $u_r$  at  $r = 0.8r_o$  with flow arrows on that surface superposed, and  $B_r$  at  $r = r_o$  for the parameters  $Ra = 750$ ,  $Ra_i = 78$ ,  $Ra_H = 2520$ . The ranges of values for the radial velocity are  $[-498.9, 310.4]$  and those for the magnetic field are  $[-1.78, 2.19]$ . (c) & (d): The same plots but for  $Ra = 125$ ,  $q = 8$  and  $Ra_H = 194$ . The range of values for the radial velocity is  $[-883.5, 403.7]$  and that for the magnetic field is  $[-6.4, 6.09]$ . Positive values are shown in red and negative values in blue (see the online version for colour).